Time-Resolved Contrast-Enhanced 3D MR Angiography

Frank R. Korosec, Richard Frayne, Thomas M. Grist, Charles A. Mistretta

An MR angiographic technique, referred to as 3D TRICKS (3D time-resolved imaging of contrast kinetics) has been developed. This technique combines and extends to 3D imaging several previously published elements. These elements include an increased sampling rate for lower spatial frequencies, temporal interpolation of *k*-space views, and zero-filling in the slice-encoding dimension. When appropriately combined, these elements permit reconstruction of a series of 3D image sets having an effective temporal frame rate of one volume every 2–6 s. Acquiring a temporal series of images offers advantages over the current contrast-enhanced 3D MRA techniques in that it i) increases the likelihood that an arterial-only 3D image set will be obtained, ii) permits the passage of the contrast agent to be observed, and iii) allows temporal-processing techniques to be applied to yield additional information, or improve image quality.

Key words: MR angiography; time-resolved MR imaging; contrast-enhanced MR imaging; rapid 3D MR imaging.

INTRODUCTION

Recently a number of groups, including our own, have had encouraging results using intravenous contrast agent in conjunction with MRA, particularly in the abdomen and the lower extremities (1–11). In these techniques, contrast between blood and stationary tissues is achieved by injecting a T_1-shortening contrast agent into the blood stream. When imaged by using a short *TR*, short *TE* gradient-echo sequence, the blood appears very bright and the stationary tissues appear dark. Vascular images acquired by using contrast-enhanced 3D MRA techniques have an inherently high signal-to-noise ratio, and thus are affected very little by many of the flow-related artifacts that reduce the sensitivity and specificity of current MRA techniques (12). Because of the high signal-to-noise ratio and the relative lack of flow-related artifacts in these images, they have an appearance similar to those obtained by using digital subtraction angiography (DSA).

Current contrast-enhanced 3D MR angiographic techniques yield excellent images of the arteries if the center of *k*-space is acquired during peak concentration of the contrast agent in the arteries. Obtaining high quality images, however, requires appropriate timing of the injection of the contrast agent relative to the start of image acquisition. If the center of *k*-space is acquired too early, maximum signal in the arteries will not be achieved, and if the center of *k*-space is acquired too late, the veins will be enhanced, causing the arteries to be obscured. Another drawback of current contrast-enhanced 3D methods is that they permit acquisition of only a single high quality scan, because image quality on subsequent scans is compromised by the residual contrast agent remaining from the first injection, which causes veins and stationary tissues to be enhanced. Also, current contrast-enhanced techniques do not reveal any information regarding the passage of the contrast agent.

We have developed a time-resolved, contrast-enhanced, 3D MR angiographic technique (3D TRICKS - 3D time-resolved imaging of contrast kinetics) that repeatedly acquires images from a volume during the passage of a contrast agent. With the appropriate choice of parameters, acquisition of multiple 3D image sets can be completed in a single breath-hold. Because this technique images the passage of the contrast agent, it increases the probability that a 3D image set showing only arteries will be obtained. The technique also provides information on the bolus transit time, which is an indicator of blood flow rate. In addition, it permits the uptake of the contrast agent by the organs to be observed. The rate of uptake has the potential to yield information regarding the physiological effects of the pathology. Also, because a series of time-resolved images is acquired, many of the postprocessing methods used with DSA and 2D time-resolved MR such as mask mode subtraction, simple matched filtering, and Eigen filtering (13, 14), can be applied to enhance the information content or quality of the images.

Several previously published techniques that improve the effective temporal resolution of MR images are employed in 3D TRICKS. These include not sampling all of the high spatial frequencies for every time frame, sharing data among time frames, and temporally interpolating between acquired blocks of data to determine values for uncollected data. "Keyhole" imaging (15) is an example of a method that provides improved temporal resolution by acquiring the high spatial frequency information less frequently than the low spatial frequency information. The keyhole technique has been generalized in the BRISK (block regional interpolation scheme for *k*-space) algorithm (16), which schedules the acquisition of *k*-space based on the temporal characteristics of the object being imaged. The BRISK technique was illustrated in the context of 2D gated cardiac imaging and used Fourier interpolation to fill in missing views. Sharing of views among multiple time frames and employing a sliding window during reconstruction is a strategy that has been used in MR fluoroscopy (17) and has recently been applied in connection with rapid 2D spiral scanning (18, 19).

MRM 36:345–351 (1996)

From the Departments of Radiology and Medical Physics, University of Wisconsin - Madison, Madison, Wisconsin.

Address correspondence to: Frank Korosec, Ph.D., UW Hospital and Clinics, Department of Radiology, E3/311, 600 Highland Avenue, Madison, WI 53792-3252.

Received March 8, 1996; revised May 8, 1996; accepted May 24, 1996.

This work was supported in part by NIH grants #R01 HL 52747 and R01 HL 51370, and a grant from the Whittaker Foundation (F.R.K.); by a Heart and Stroke Foundation of Canada Fellowship (R.F.); and in part by NIH grant #K08 HL 02848 (T.M.G.).

0740-3194/96 $3.00

Temporal interpolation has been used in 2D cine techniques to improve temporal resolution and as a means of approximating data for points in the cardiac cycle from which no data were acquired (20). An additional method employed in the 3D TRICKS technique to improve temporal resolution, is zero-filling (21) in the slice-encoding dimension. Typically, half the slice-encoding data are acquired, and half are zero-filled for a reduction in scan time by factor of 2.

METHODS

Rapid acquisition of multiple 3D image sets was made possible by not collecting all of the *k*-space data for every reconstructed time frame. Instead, the lower spatial frequencies, because they contribute most significantly to the image content, were acquired more frequently than the higher spatial frequencies (16, 18, 19, 22), and the missing data were estimated by interpolating between data that were collected.

To better understand the acquisition strategy employed, consider 3D *k*-space as being divided into four sections and labeled as shown in Fig. 1. (Although many *k*-space divisions are possible, we chose this division for the initial evaluation because of its simplicity and ease of implementation.) For this work, the higher spatial frequencies in the k_y dimension (labeled B, C, and D in Fig. 1) were sampled three times less frequently than the lower spatial frequencies (labeled A in Fig. 1). The data

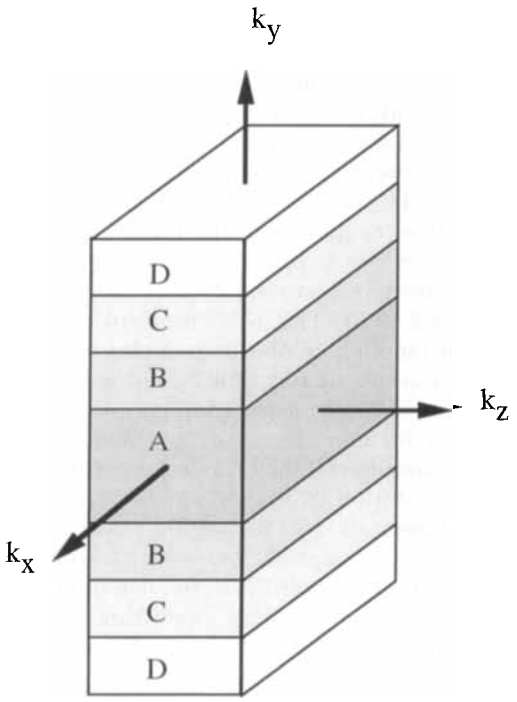

Fig. 1 Schematic showing the division of *k*-space into four equal sections labeled A, B, C, and D. Although this division was used in this initial work, other divisions in both k_y and k_z could be used. In this figure, k_x is the frequency-encoding direction, k_y is the phase-encoding direction, and k_z is the slice-encoding direction. If the total number of k_y = 128, the divisions would be as follows: D (k_y = 1–16, 113–128), C (k_y = 17–32, 97–112), B (k_y = 33–48, 81–96), A (k_y = 49–64, 65–80).

were collected in the following order: D, A, C, A, B, A. This cycle was repeated throughout the scan. In addition, before the first cycle and after the last cycle, D, C, B, and A sections were acquired. Thus, for a scan in which the cycle was repeated two times, the acquisition order was D_1, C_2, B_3, A_4, D_5, A_6, C_7, A_8, B_9, A_{10}, D_{11}, A_{12}, C_{13}, A_{14}, B_{15}, A_{16}, D_{17}, C_{18}, B_{19}, A_{20}, where the subscript numbers indicate the time interval in which each section was acquired (see Fig. 2). In collecting the data for the images shown in this work, the cycle was repeated four times (i.e., a total of 32 sections were acquired).

Figure 2 schematically shows the order in which the *k*-space sections would be acquired for the two-cycle example described above, and how they would be shared and interpolated to reconstruct the temporally resolved image volumes. In the present implementation, a 3D image set was reconstructed for each time interval that is straddled by a B, C, and D pair, as shown in Fig. 2, where a time interval is defined as the time required to sample each section of *k*-space. Data that were not collected were estimated by linearly interpolating (in time) between the sections that were acquired. For the example shown in Fig. 2, an image at Time frame 5 was reconstructed using the data $\{A_8, I(B_3,B_9), I(C_7,C_{13}), I(D_5,D_{11})\}$, where I() denotes linear interpolation. Acquiring D, C, B, and A sections before the first cycle and after the last cycle increased the number of time frames that could be reconstructed because it provided end points between which data could be interpolated.

For this work, the data were acquired on a 1.5 T MR scanner (Signa; General Electric Medical Systems, Waukesha, WI) by using a modified 3D gradient-echo pulse sequence. The time required to collect each section of *k*-space ranged from 2 to 8 s, depending on the number of phase encodings and slice encodings acquired, and the *TR* of the sequence. For k_y = 96 (phase encodings), k_z = 16 (slice encodings), and a *TR* of 10 ms, acquisition of each of the four sections of *k*-space required 3.8 s. Zero-filling (21) was used to increase the number of k_y points to 256, and to double the number of k_z points.

To date, we have used 3D TRICKS on 5 volunteers and 7 patients, and have obtained 20 temporally resolved contrast-enhanced 3D image sets. Multiple locations were imaged in 6 subjects. The contrast agent Gadodiamide (Omniscan; Nycomed, Princeton, NJ) was manually injected into each of the subjects at a rate of 3–5 ml/s.

Reconstruction of the image sets was performed on an off-line workstation (SparcStation20; Sun MicroSystems, Mountain View, CA). After reconstruction, a Maximum intensity pixel (MIP) image was formed for each 3D image set (time frame). These MIP images were used to identify the time frames that contained the vascular information of interest. If the vessel-to-stationary-tissue contrast was sufficient, additional MIP reprojections were formed by using the pertinent image sets. If the vessel-to-stationary-tissue contrast was insufficient, or if venous signal interfered with arterial signal, appropriate image sets were subtracted to eliminate the unwanted signal.

When performing subtraction, it was necessary to use the individual source images rather than MIP projections of the data, because the MIP process is non-

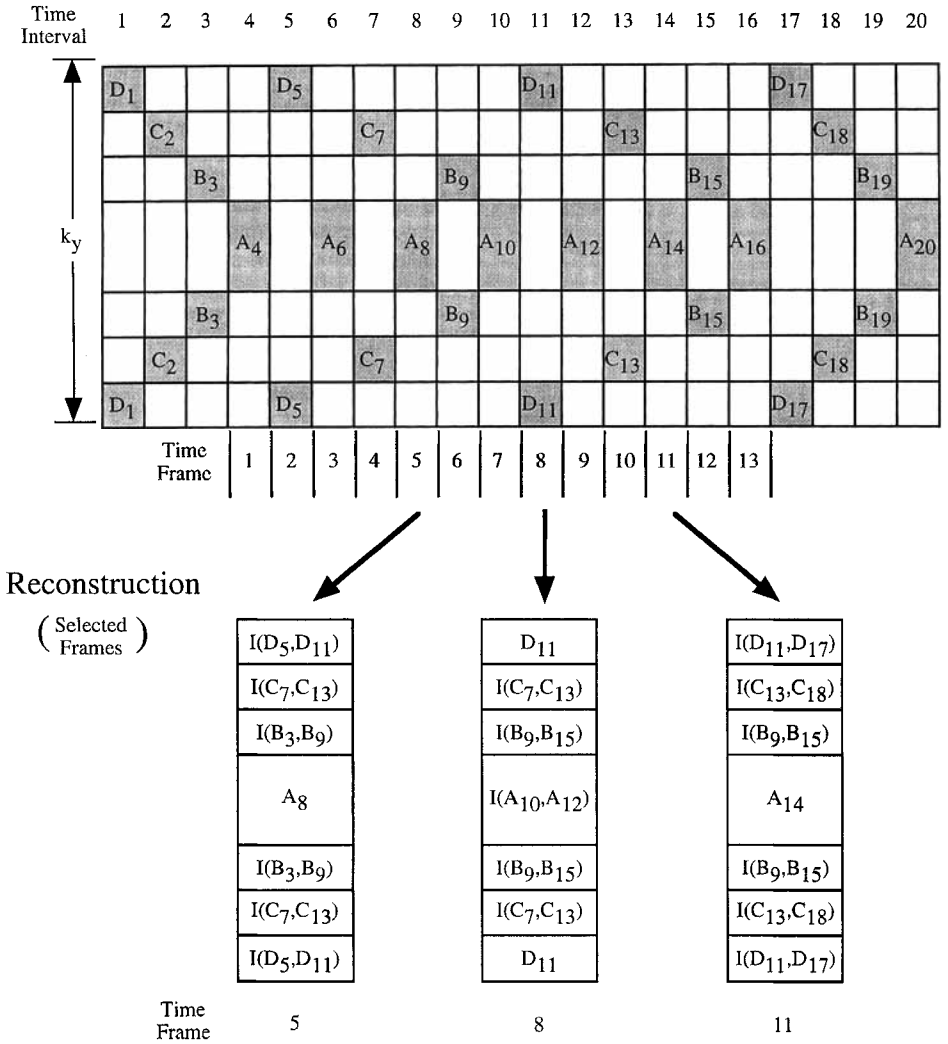

Fig. 2 Schematic showing the acquisition order for the various sections of *k*-space, and the interpolation strategy used to reconstruct the temporally resolved 3D image sets. The top part of the figure shows which section of *k*-space was acquired in each time interval. (See Fig. 1 for the breakdown and labeling of 3D *k*-space used in this work.) The subscript number on each of the section labels indicates the time interval in which the section was acquired. Shown here are only two cycles of D, A, C, A, B, A. For this example, image volumes corresponding to time intervals 4 through 16 would be reconstructed, and would be denoted as Time frames 1 through 13. The gray boxes indicate data that were collected, whereas the white boxes indicate data that were not collected but were needed to reconstruct the various time frames. The bottom part of the figure demonstrates how missing data were calculated by linearly interpolating between the nearest pairs of data that were collected. Data for Time frames 5, 8, and 11 are shown. Data for the remaining time frames were calculated in a similar manner.

linear. To illustrate the necessity to use the source images rather than the MIP images, consider the result of a subtraction in which a later venous-only MIP image is subtracted from an earlier arterial and venous MIP image. The difference MIP image would suppress the venous anatomy, but would not reveal structures that were obscured by the veins, because this information is not contained in the MIP images. Thus, subtracting the MIP images would yield images without veins, but instead of revealing what was masked by the veins, the signal in regions previously occupied by veins would be zero. Because of this, subtraction was performed on the individual slices before formation of a projection image using methods such as MIP or DART (data adaptive reprojection technique) (23).

RESULTS

In Figs. 3–5 we present representative angiograms acquired by using the 3D TRICKS technique. Figure 3 shows MIP images of three of the 27 3D image sets acquired from the torso of a female volunteer. Parameters were: field of view (FOV) = 44 × 22 × 6.4 cm, tip/*TR*/*TE* = 60°/10.8 ms/1.9 ms, acquisition matrix = 308 × 128 × 16, reconstruction matrix = 512 × 256 × 32, reconstructed voxel size = 0.86 × 0.86 × 2.0 mm, time between frames = 5.6 s, coil = torso phased-array, and Gadodiamide dose = 35 ml (0.3 mmol/kg). The volunteer began holding her breath about 20 s into the scan, and held it for as long as she could. She then breathed and held her breath again for the remainder of the scan. Injection of the contrast agent began at the same time as the first breath-hold. The major blood vessels from above the heart to below the aorto-iliac bifurcation are clearly visualized, including some of the pulmonary vessels. In addition, the passage of the contrast agent is clearly seen over the time frames shown. Notice how temporal resolution allows the renal arteries to be clearly seen (Fig. 3b) without overlap from the renal veins and inferior vena cava. In later frames, the renal veins obscure visualization of the renal arteries (Fig. 3c). If this were not a time-resolved acquisition, and Fig. 3c were the only image obtained, diagnosis of renal artery disease would be difficult from only this data. The data from Fig. 3c is

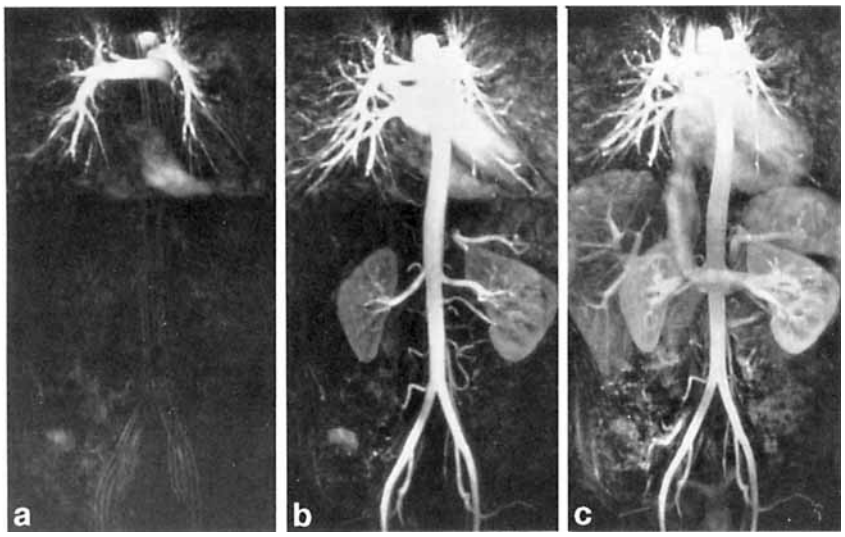

Fig. 3 MIP projections of 3 of 27 temporally resolved volumes acquired from a female volunteer using 3D TRICKS. The images show a coronal view of the vessels in the abdomen, thorax, and pelvis. An early phase (a) demonstrates the presence of contrast agent in the pulmonary vessels. An intermediate phase (b) clearly demonstrates the aorta and renal arteries without interference from veins. A later phase (c) shows the presence of contrast medium in the renal veins, making visualization of the renal arteries very difficult. The very bright signal in the pulmonary vessels and the heart are due to the use of a surface coil (torso phased-array).

representative of that which would be obtained if a non-time-resolved image set were acquired too late after the injection of the contrast agent. The enhancement of the edges of the aorta in Fig. 3a results because the contrast is present during the acquisition of only the high spatial frequencies of this time frame. This would occur, for example, in Time frame 5 (see Fig. 2) if the contrast agent were not present during the acquisition of section A_8, but arrived before the acquisition of section D_{11}. (Other interpolation methods can be employed to reduce or eliminate this effect.)

Figures 4a–4c show MIP projections of three of 27 volumes acquired using a sagittal acquisition centered on the right carotid artery of a female volunteer. Parameters were: FOV = 24 × 12 × 3.2 cm, tip/*TR*/*TE* = 60°/10.9 ms/2.0 ms, acquisition matrix = 308 × 96 × 8, reconstruction matrix = 512 × 256 × 16, reconstructed voxel size = 0.47 × 0.47 × 2.0 mm, time between frames = 2.1 s, coil = quadrature head/neck/vascular, and Gadodiamide dose = 15 ml (0.1 mmol/kg). In non-time-resolved 3D contrast-enhanced imaging, it is difficult to image the carotid arteries without interference from the jugular veins due to the rapid arterial-to-venous transit times in this region. For the images shown here, the time between reconstructed frames is 2.1 s, permitting three arterial-only frames to be acquired. In addition, Fig. 4d demonstrates the effectiveness of subtracting a venous-only frame (Fig. 4c) from an arterial and venous frame (Fig. 4b) to eliminate the venous signal, thereby, providing an additional arterial-only frame.

Figure 5a shows an MIP image of one time frame acquired from the thighs of a male patient. This image was acquired during a second injection of contrast agent. The pelvis was imaged during the first injection. Parameters were: FOV = 44 × 22 × 5.8 cm, tip/*TR*/*TE* = 60°/10.8 ms/1.9 ms, acquisition matrix = 308 × 128 × 16, reconstruction matrix = 512 × 256 × 32, reconstructed voxel size = 0.86 × 0.86 × 1.8 mm, time between frames = 5.7 s, coil = torso phased-array, and Gadodiamide dose = 30 ml (0.2 mmol/kg). The stationary tissues are bright in all of the time frames indicating that the contrast from the first injection has perfused into them. The contrast agent has also accumulated in the bladder, causing it to appear bright in the images. Wrap-around artifacts (arrows) are present in this image because of the reduced FOV used in the right/left direction. Figure 5b is an MIP projection through the same images used to produce the MIP image in Fig. 5a, after images from an earlier, precontrast, data set have been subtracted from them. Note the subtraction eliminates the bladder and the stationary tissues (including those that have aliased), permitting the arteries to be clearly visualized. All venous signals resulting from the presence of residual contrast agent remaining from the first injection are also eliminated. Figure 5c is an earlier, postcontrast, time frame from the same scan (again after subtraction of an earlier, precontrast, time frame) showing the late arrival of the contrast agent in the left iliac artery, resulting from a stenosis in this artery (superior to the region shown).

DISCUSSION

Initial applications of the time-resolved, contrast-enhanced 3D MRA technique show encouraging results. The technique maintains all of the benefits of non-time-resolved contrast-enhanced 3D MRA (1, 3, 9, 10), including excellent delineation of the vessels and a reduced sensitivity to many of the flow-related artifacts that have historically compromised MR angiograms. The 3D TRICKS technique offers additional advantages due to its ability to provide temporal information. These advantages are discussed below.

In peripheral vessels, non-time-resolved contrast-enhanced 3D MRA has been used with much success (1, 8, 11), providing excellent images of the distal aorta and the proximal iliac and femoral arteries. The principal limitation of the non-time-resolved contrast-enhanced 3D MRA technique, as currently implemented, is that it permits only a single location to be imaged. If a second location is imaged, the presence of residual contrast agent from the previous injection causes the signals from veins and stationary tissues to be markedly enhanced, compromising image quality, and making arterial-venous discrimination difficult. With the 3D TRICKS technique,

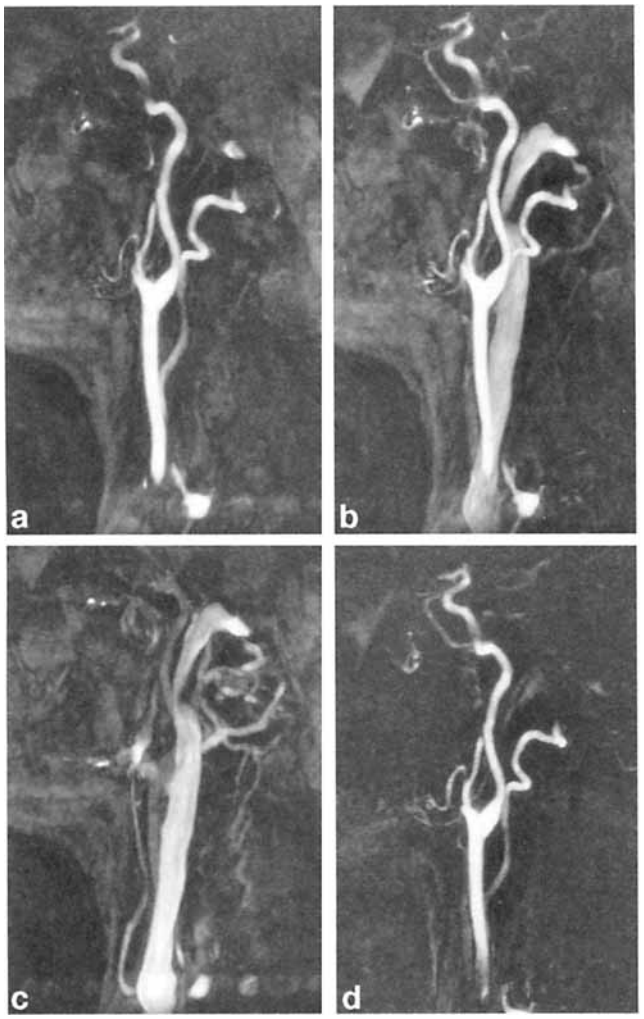

Fig. 4 MIP projections from 3 of 27 temporally resolved volumes acquired from the neck of a female volunteer by using 3D TRICKS. The images show a sagittal view of the left carotid artery and jugular vein. The images demonstrate (a) an early phase showing the presence of contrast medium in the carotid artery, (b) an intermediate phase showing the presence of contrast medium in both the carotid artery and the jugular vein, and (c) a late phase showing the presence of contrast medium in only the jugular vein. (d) An arterial-only image obtained by subtracting the source images used to produce (c) from the source images used to produce (b), and applying the MIP algorithm to the resulting images.

multiple locations can be imaged using multiple injections, because enhanced signals from veins and stationary tissues can be eliminated by using temporal postprocessing techniques as shown in Fig. 5.

An additional consideration in imaging the peripheral vessels is that, in patients with significant occlusive disease, there can be a marked difference in the arrival times of the contrast agent in the diseased and nondiseased vessels. Thus, with a non-time-resolved acquisition, it can be very difficult to choose the appropriate delay between contrast agent infusion and image acquisition. This problem is circumvented in conventional contrast angiography by obtaining multiple time frames after the injection of iodinated contrast agent. The 3D TRICKS technique also accommodates variations in the timing of the arrival of contrast in diseased versus nondiseased vessels by acquiring multiple time frames after the injection of the contrast agent (as shown in Figs. 5b and 5c). By acquiring time-resolved images, the delay in the arrival of the contrast agent may be quantified, and perhaps used to aid the diagnosis.

Non-time-resolved contrast-enhanced 3D MR angiography, as it is currently applied, can provide an exact measurement of the stenosis lumen diameter due to reduced sensitivity of the technique to complex flow-related signal loss (24). However, non-time-resolved contrast-enhanced 3D methods have not been applied, for example, to the carotid arteries because the rapid enhancement of the jugular veins prevents clear observation of the carotid arteries. The 3D TRICKS technique provides several phases in which the carotid arteries are shown without any interference from veins (an example is shown in Fig. 4a). In addition, subtraction of later phases can be used to eliminate venous signal from some of the intermediate phases to yield additional artery-only images as shown in Fig. 4d.

3D TRICKS, when used to image the passage of an intravenous injection of a contrast agent, can be compared with IV-DSA and the more recently developed IV-CTA (computed tomography angiography) (25). IV-CTA has begun to be investigated with encouraging results (26). Drawbacks of the technique include the use of ionizing radiation, the toxicity of the contrast material (27), and occasional problems with bolus timing (28). Although CTA provides a 3D data set that permits formation of additional projections (29), there is no opportunity for generating a temporal series of images for following the time course of the contrast material as there is in 3D TRICKS. This ability frequently is helpful for separation of closely wound arteries and veins, as well as evaluating the effect of vascular disease on tissue perfusion. The limitations of IV-DSA include the use of ionizing radiation, the requirement for large quantities of iodinated contrast material, and the inability to reproject the acquired data at arbitrary angles.

Although not employed in this initial work, the FOV could be reduced to enhance temporal resolution (decrease the number of acquired k_y points) without effects of spatial wrap-around by using the reduced-FOV method proposed by Fredrickson and Pelc (30). In the case of 3D TRICKS, assuming even-numbered views are collected during the ongoing acquisition, a set of complementary odd-numbered views could be acquired once at the beginning of the acquisition sequence, and possibly again at the end of the sequence. This data could then be combined as described by Fredrickson and Pelc (30) to eliminate wrap-around artifacts from nonenhancing tissues. Elimination of wrap-around artifacts from nonenhancing tissues can also be achieved (without using the reduced-FOV algorithm) by subtracting a precontrast or a late postcontrast time frame from a fully enhanced arterial time frame (as shown in Fig. 5b). Both subtraction and the small-FOV algorithm will eliminate aliased signal, provided that the aliased signal is time independent.

Because each *k*-space section is acquired in a time of about 2–6 s, and each image set is reconstructed using a temporal aperture on the order of several seconds, mo-

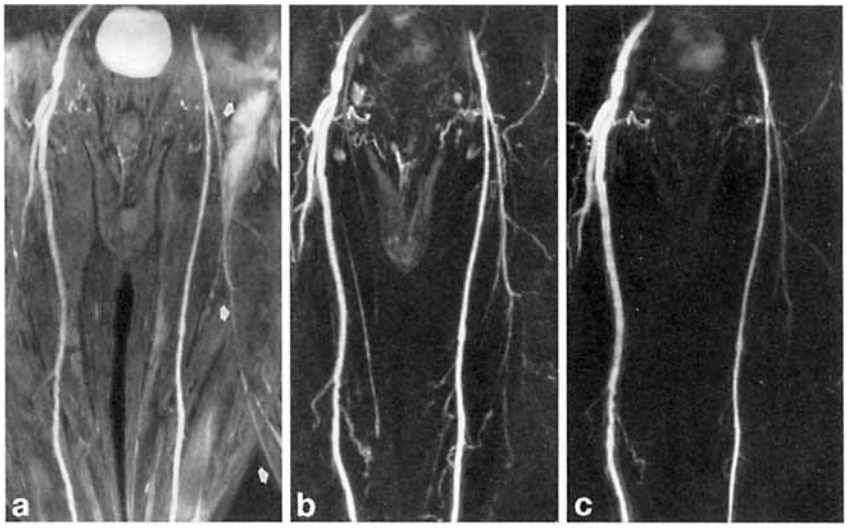

Fig. 5 (a) A coronal MIP image of 1 of 27 time frames of the thighs of a patient acquired by using the 3D TRICKS technique. This image was acquired during the second injection of the contrast agent. (The pelvis was imaged during the first injection.) Note the bright signal from the stationary tissues, indicating that the contrast from the first injection has diffused into and remained in these tissues. Note also the wrap-around artifact (arrows) resulting from the small FOV. The source images from an earlier, precontrast time frame, were subtracted from the source images used in (a), and an MIP reprojection of the resulting images is shown in (b). Note that the stationary tissues are eliminated, as is the wrap-around artifact from the stationary tissues, permitting the arteries to be well visualized. Note also the absence of venous signal. (c) An earlier postcontrast time frame, showing the late arrival of the contrast agent in the left iliac artery, caused by a stenosis in this artery.

tion (such as respiration) causes only a temporary disruption of image quality, similar to that observed in MR fluoroscopy. This motion robustness is reminiscent of the recursive DSA filters still used for many current subtractive fluoroscopic procedures. These temporal characteristics also make the 3D TRICKS sequence robust in the presence of variations in the shape and timing of the contrast-pass curve as we have confirmed in simulations (31). Additionally, if motion between successive images is small, then the full suite of temporal processing schemes, previously investigated in connection with DSA and time-resolved 2D MR, such as mask mode subtraction, simple matched filtering, and Eigen filtering, can be used to obtain further information or improved image quality.

CONCLUSIONS

We have developed and implemented a time-resolved, contrast-enhanced, 3D MR imaging technique that permits rapid acquisition of temporally resolved 3D image sets. This technique, referred to as 3D TRICKS, is a novel combination of well understood data acquisition and data reconstruction concepts. These concepts include: variable rate *k*-space sampling, temporal interpolation, and zero-filling in the slice dimension. When appropriately combined, these concepts decrease the interval between frames without incurring significant image artifacts.

The 3D TRICKS technique, when used in conjunction with the administration of a contrast agent, permits the acquisition of multiple frames during the passage of the contrast agent, making less critical the issue of the timing of the scan relative to the injection of the contrast agent. The 3D TRICKS technique provides a robust and time-efficient MR angiographic method that i) provides temporal information, ii) has inherently high signal-to-noise, iii) can be acquired in any orientation, independent of the direction of blood flow, iv) preserves signal in regions of complex flow, v) minimizes motion artifacts, vi) is insensitive to variation in the shape and timing of the contrast bolus, vii) produces high-quality volume angiograms that can be reformatted or reprojected, and, viii) allows the application of a variety of temporal postprocessing techniques.

Although applied here to angiographic imaging, the 3D TRICKS acquisition method can be applied to other situations requiring imaging of dynamic processes, such as investigating joint movement, or attempting to classify tumors by their rate of uptake of contrast agent.

REFERENCES

1. S. V. Lossef, S. S. Rajan, R. H. Patt, M. Carvlin, D. Calcagno, M. N. Gomes, K. H. Barth, Gadolinium-enhanced magnitude contrast MR angiography of popliteal and tibial arteries. *Radiology* **184**, 349–355 (1992).
2. V. M. Runge, J. E. Kirsch, C. Lee, Contrast-enhanced MR angiography. *J. Magn. Reson. Imaging* **3**, 233–239 (1993).
3. M. R. Prince, E. K. Yucel, J. A. Kaufman, D. C. Harrison, S. C. Geller, Dynamic gadolinium-enhanced three-dimensional abdominal MR arteriography. *J. Magn. Reson. Imaging* **3**, 877–881 (1993).
4. W. Lin, E. M. Haacke, A. S. Smith, M. E. Clampitt, Gadolinium-enhanced high resolution MR angiography with adaptive vessel tracking: preliminary results in the intracranial circulation. *J. Magn. Reson. Imaging* **2**, 277–284 (1992).
5. G. Sze, S. N. Goldberg, Y. Kawamura, Comparison of bolus and constant infusion methods of gadolinium administration in MR angiography. *AJNR* **15**, 909–912 (1994).
6. G. A. Holland, L. Dougherty, B. L. Greenman, R. A. Baum, J. P. Carpenter, M. D. Schnall, M. Gilfeather, L. Axel, Ultrafast 3D time-of-flight MR angiography with gadolinium of the abdominal aorta and the visceral vessels performed in a breath-hold: preliminary experience, *in* "Proc., SMR, Third Annual Meeting, 1995," p. 77.

7. D. Revel, P. Loubeyre, A. Delignette, P. Douek, M. Amiel, Contrast-enhanced magnetic resonance tomoangiography: a new imaging technique for studying thoracic great vessels. *Magn. Reson. Imaging* **11,** 1101–1105 (1993).
8. P. C. Douek, D. Revel, S. Chazel, B. Falise, J. Villard, M. Amiel, Fast MR angiography of the aotoiliac arteries and arteries of the lower extremity: value of bolus-enhanced, whole-volume subtraction technique. *AJR* **165,** 431–437 (1995).
9. P. M. Rodgers, J. Ward, C. J. Baudouin, J. P. Ridgway, P. J. Robinson, Dynamic contrast-enhanced imaging of the portal venous system: comparison with x-ray angiography. *Radiology* **191,** 741–745 (1994).
10. M. R. Prince. Gadolinium-enhanced MR aortography. *Radiology* **191,** 155–164 (1994).
11. J. S. Swan, T. M. Grist, F. R. Korosec, T. W. Kennell, J. R. Hoch, D. M. Heisey, MR angiography of the pelvis with breath-held gadolinium-enhanced 3D TOF using *k*-space zero-filling and a contrast timing scan, *in* "Proc., SMR, Fourth Annual Meeting, 1996," p. 744.
12. R. R. Edelman, H. P. Mattle, D. J. Atkinson, H. M. Hoogewoud, MR angiography. *AJR* **154,** 937–946 (1990).
13. Y. Wang, D. M. Weber, F. R. Korosec, C. A. Mistretta, T. M. Grist, J. S. Swan, P. A. Turski, Generalized matched filtering for time-resolved MR angiography of pulsatile flow. *Magn. Reson. Med.* **30,** 600–608 (1993).
14. A. M. Haggar, J. P. Windham, D. A. Reimann, D. O. Hearshen, J. W. Froelich, Eigenimage filtering in MR imaging: an application in the abnormal chest wall. *Magn. Reson. Med.* **11,** 85–97 (1989).
15. J. J. van Vaals, M. E. Brummer, W. T. Dixon, H. H. Tuithof, H. Engels, R. C. Nelson, B. M. Gerety, J. L. Chezmar, J. A. den Boer, "Keyhole" method for accelerating imaging of contrast agent uptake. *J. Magn. Reson. Imaging* **3,** 671–675 (1993).
16. M. Doyle, E. G. Walsh, G. G. Blackwell, G. M. Pohost, Block regional interpolation scheme for *k*-space (BRISK): a rapid cardiac imaging technique. *Magn. Reson. Med.* **33,** 163–170 (1995).
17. S. J. Riederer, T. Tasciyan, F. Farzaneh, J. N. Lee, R. C. Wright, R. J. Herfkens, MR fluoroscopy: technical feasibility. *Magn. Reson. Med.* **8,** 1–15 (1988).
18. A. B. Kerr, J. M. Pauly, C. H. Meyer, D. G. Nishimura, New strategies in spiral MR fluoroscopy, *in* "Proc., SMR, Third Annual Meeting, 1995," p. 99.
19. D. M. Spielman, J. M. Pauly, C. H. Meyer, Magnetic resonance fluoroscopy using spirals with variable sampling densities. *Magn. Reson. Med.* **34,** 388–394 (1995).
20. N. J. Pelc, R. J. Herfkens, A. Shimakawa, D. R. Enzmann, Phase contrast cine magnetic resonance imaging. *Magn. Reson. Q.* **7,** 229–254 (1991).
21. Y. P. Du, D. L. Parker, W. L. Davis, G. Cao, Reduction of partial-volume artifacts with zero-filled interpolation in three-dimensional MR angiography. *J. Magn. Reson. Imaging* **4,** 733–741 (1994).
22. J. A. Polzin, R. Frayne, T. M. Grist, C. A. Mistretta, Phase-contrast flow measurements with variable rate *k*-space sampling, *in* "Proc., SMR, Third Annual Meeting, 1995," p. 593.
23. F. R. Korosec, D. M. Weber, C. A. Mistretta, P. A. Turski, M. A. Bernstein, A data adaptive reprojection technique for MR angiography. *Magn. Reson. Med.* **24,** 262–274 (1992).
24. S. N. Urchuck, D. B. Plewes, Mechanisms of flow-induced signal loss in MR angiography. *J. Magn. Reson. Imaging* **2,** 453–462 (1992).
25. W. A. Kalender, W. Seissler, E. Klotz, P. Vock, Spiral volumetric CT with single-breath-hold technique, continuos transport, and continuous scanner rotation. *Radiology* **176,** 181–183 (1990).
26. G. D. Rubin, M. D. Dake, C. P. Semba, Current status of three-dimensional spiral CT scanning for imaging the vasculature. *Radiol. Clin. North Am.* **33,** 51–70 (1995).
27. G. D. Rubin, M. D. Dake, S. A. Napel, C. H. McDonell, R. B. Jeffery, Three-dimensional spiral CT angiography of the abdomen: initial clinical experience. *Radiology* **186,** 147–152 (1993).
28. L. van Hoe, G. Marchal, A. L. Baert, S. Gryspeerdt, L. Mertens, Determination of scan delay time in spiral CT-angiography: utility of a test bolus injection. *J. Comput. Assist. Tomogr.* **19,** 216–220 (1995).
29. S. Napel, M. P. Marks, G. D. Rubin, M. D. Dake, C. H. McDonnell, S. M. Song, D. R. Enzmann, R. B. Jeffery Jr., CT angiography with spiral CT and maximum intensity projection. *Radiology* **185,** 607–610 (1992).
30. J. O. Fredrickson, N. J. Pelc, Temporal resolution improvement in dynamic imaging, *in* "Proc., SMR, Third Annual Meeting, 1995," p. 197.
31. C. A. Mistretta, T. M. Grist, R. Frayne, F. R. Korosec, J. A. Polzin, Simulation of a breath-hold method for time-resolved 3D contrast imaging, *in* "Proc., SMR, Fourth Annual Meeting, 1996," p. 1498.